DOPPLER MEASUREMENTS OF THE IONOSPHERE ON THE OCCASION OF THE APOLLO-SOYUZ TEST PROJECT

Part II

RAY H. GAY and MARIO D. GROSSI

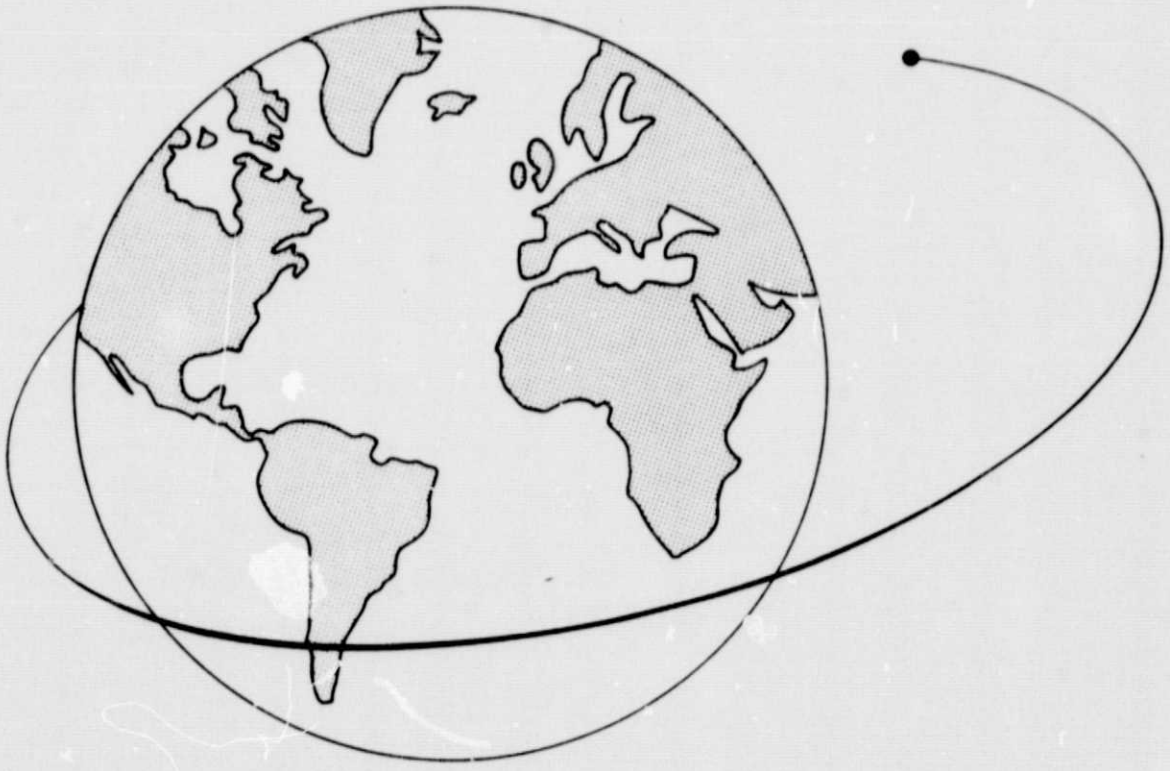

Smithsonian Astrophysical Observatory
SPECIAL REPORT 367

TABLE OF CONTENTS

ILLUSTRATIONS

TABLE

ABSTRACT

The preparation of the analytical approach and of the related software to be used in the inversion of the differential and rotating doppler data that the ionospheric experiment of the Apollo-Soyuz Test Project (ASTP) will obtain has been recently completed. These data will be collected in space-to-space paths (between the ASTP Docking Module (DM) and the Apollo Command Service Module that will orbit both at a height of 221 km, at a relative distance of 300 km) and in space-to-ground paths (between the DM and ground). The doppler links will operate at 162 and 324 MHz and will have an accuracy better than 3 mHz over 10-sec integration time. The ASTP Mission is scheduled for summer 1975. While waiting for the actual experiment data, the inversion approach has been tested with the "dummy" data obtained with a computer simulation. We found that a measurement accuracy of 1 to 10% in the value of the horizontal electron density gradient at 221-km altitude can be achieved, in space-to-space paths. For space-to-ground paths near the orbital plane, we have identified and compensated for possible effects of the horizontal gradients on the received differential doppler shifts. In the two cases we have considered, it was possible to reduce the gradient-associated errors in the inversion that leads to the columnar electron content by approximately one-half. Accuracies of 5 to 10% in columnar electron content are achievable, with this gradient-compensation technique.

DOPPLER MEASUREMENTS OF THE IONOSPHERE ON THE OCCASION OF THE APOLLO-SOYUZ TEST PROJECT

Part II: Inversion of Differential and Rotating Doppler Shifts*

Ray H. Gay and Mario D. Grossi

1. INTRODUCTION

The forthcoming Apollo-Soyuz Test Project (ASTP) gives us an opportunity to collect valuable observations of the columnar electron content in the ionosphere at an altitude of 221 km and below. In addition, doppler measurements between the Apollo-Soyuz docking module (DM) and the command service module (CSM) make it possible to obtain relatively continuous signatures of the electron-content gradient in the spacecraft's orbit over a 24-hour period. After determining the aloft gradient, we can then consider the effect of electron-density horizontal gradients on the DM-to-ground differential doppler shift. Although the total gradient contribution is along the ray trajectory, accurate measurements of the gradient at the spacecraft altitude may be fitted to existing ionospheric models in order to improve the description of gradient integrals along the spacecraft-to-ground path.

The detection of mass concentrations in the earth from measurements of small accelerations between the DM and the CSM is dependent on an accurate determination of the ionospheric doppler shift in the DM/CSM radio link. A 1-Hz differential doppler shift is possible in the presence of large gradients and corresponds roughly to an apparent relative velocity of 1/3 m sec^{-1} between the receiver and the transmitter. Such a value is 100 to 1000 times as large as the expected mascon doppler signature. In nighttime regions, where the horizontal gradients are small, the gravitational and ionospheric doppler magnitudes are comparable. The use of two oscillators operating coherently at different frequencies enables the dynamical part of the doppler shift to be isolated from the ionospheric component, but the determination of the DM/CSM gradient and resulting individual frequency shifts due to the ionosphere must be quite accurate in order to maintain the integrity of the residual mascon-induced doppler shift at the 2- to 3-mHz level.

---

*This report covers the inversion of differential and rotating doppler shifts (Part II). Part I (SAO Special Report No. 366) covers the computer simulation of the ionospheric experiment results.

This research was supported by NASA under contract NAS 9-13837 to the Smithsonian Astrophysical Observatory.

2. REDUCTION OF DM/CSM DOPPLER SHIFT AND RECOVERY OF HORIZONTAL ELECTRON-DENSITY GRADIENTS

First, it is informative to develop an approximate expression for the differential doppler shift between the two spacecraft as a function of the electron density along the ray path. The negative phase-path defect,

$$L = P - \rho \quad ,$$

is the difference between the straight-line distance ρ and the radio length P of the ray path. The phase-path length is related to the refractive index μ by

$$P = \int_A^B \mu \, dS \quad , \tag{1}$$

where dS is an element of length along the curvilinear ray path from point A to point B in space.

For the ASTP experiment, the instrument frequencies (f_1 = 324 MHz, f_2 = 162 MHz) are much higher than either the electron gyrofrequency f_H or the critical or plasma frequency f_0 in the ionosphere. For a typical electron density of 10^5 el cc^{-1} and a magnetic-field strength of 0.28 Oe, f_H = 0.8 MHz and f_0 = 2.8 MHz.

Neglecting collisions and the earth's magnetic field, we can write for the refractive index (Kelso, 1964, Chap. 5)

$$\mu = 1 - \frac{e^2 N}{2\pi m f^2} \quad ,$$

where e and m are the electron charge and the rest mass, respectively, and N is the electron density in el cc^{-1}. In mks units, we have

$$\mu \simeq 1 - \frac{40.3\,N}{f^2} \quad ,$$

where f is in Hertz.

The expression for the total doppler shift between the transmitter A and a removed point B is

$$\dot{\Phi} = \frac{\dot{P}}{\lambda} = \frac{1}{\lambda}\frac{d}{dt}\int_A^B (\mu - 1)\, dS \quad . \tag{2}$$

When the range ρ differs insignificantly from the arc length $\int_A^B dS$, the two quantities $d\rho/dt$ and $(d/dt)\int_A^B dS$ can be interchanged without serious errors being introduced. In fact, the dual-frequency technique removes these terms from consideration in first-order expressions for the differential frequency shift. The differential doppler shift obtained from the coherent emission at two frequencies f_1 and f_2 is

$$\delta\dot{\Phi} = \dot{\Phi}_1 - \frac{f_1}{f_2}\dot{\Phi}_2 \quad , \tag{3}$$

and if we allow the same integration path for the two frequencies in equation (2), we can write

$$\delta\dot{\Phi} = \frac{40.3}{2\lambda_1}\left(\frac{1}{f_2^2} - \frac{1}{f_1^2}\right)\frac{d}{dt}\int_A^B N\, dS \qquad \left(\lambda_1 = \frac{c}{f_1}\right) \quad , \tag{4}$$

where the quantity $\int_A^B N\, dS$ is the total electron content per unit area between A and B. The total time derivative of $\int N\, dS$, in general, is a complicated expression involving the motion of points A and B and various partial derivatives of N; but when the doppler link is between two satellites in coplanar circular orbits, the expression is

$$\frac{d}{dt}\int_{CSM}^{DM} N\, dS = N(CSM)\, v_{CSM} - N(DM)\, v_{DM} + \int_{DM}^{CSM}\frac{\partial N}{\partial t}\, dS \quad , \tag{5}$$

where v_{CSM} and v_{DM} are the velocity components of the CSM and the DM in the direction of propagation at their respective end points of the ray path. If the X axis has its origin at the CSM and passes through the DM and if the two spacecraft are in nearly coincident circular orbits, then equation (5) becomes

$$\frac{d}{dt}\int N\, dX = [N(CSM) - N(DM)]\, v_0 + \int\frac{\partial N}{\partial t}\, dS \quad , \tag{5a}$$

where v_0 is the common orbital speed. The first term in equation (5a) can be written

$$[N(CSM) - N(DM)]\, v_0 = v_0 \frac{\Delta N}{\Delta X} \Delta X \quad ,$$

so that equation (5) is finally

$$\frac{d}{dt} \int_{CSM}^{DM} N \, dS = v_0 \frac{\overline{\partial N}}{\partial X} \Delta X + \int_{DM}^{CSM} \frac{\partial N}{\partial t} \, dX \quad , \tag{5b}$$

where $\overline{\partial N}/\partial X$ is the average gradient along the path connecting the two spacecraft, and $\partial N/\partial t$ is the temporal variation of electron density in the path. If we neglect or can otherwise account for the $\partial N/\partial t$ term, then equation (4) gives a direct measurement of the electron-density gradient at the ASTP altitude averaged over the DM/CSM separation arc.

Thus, the average horizontal gradient involved is given by

$$\frac{\overline{\partial N}}{\partial X} = \frac{\lambda_1 f_1^2 f_2^2}{40.3 \left(f_2^2 - f_1^2\right)} \frac{\delta\dot{\Phi}}{v_0 \, \Delta X} \quad . \tag{6}$$

In order to obtain a global view of the smoothed $\delta\dot{\Phi}$ in the DM/CSM path, we computed a series of phase-path lengths for each frequency at points along the orbit separated by 15° in longitude (Figure 1). The ionospheric electron-density model for summer 1975 (Odom, 1975) was used. The temporal effect of $\partial N/\partial t$ and the earth's magnetic field were excluded from the simulation. The averaged $\delta\dot{\Phi}$ between successive points along the orbit corresponding to 1200 LT, 1300 LT, ... was approximated at the midpoints of each longitude segment by simply taking $\delta\dot{\Phi} = (\Delta\Phi/\Delta \text{ long})\ (\Delta \text{ long}/\Delta t)$. These 1-hour intervals in geocentric longitude correspond to time intervals of 3.45 to 4.93 min along the orbit (whose period is ~88 min), so they represent averages of many individual 10-sec observations of the expected $\delta\dot{\Phi}$.

The expected DM/CSM differential doppler shift for an entire orbit is shown in Figure 2. The steepest gradients occur between 1030 and 1230 LT and result in a

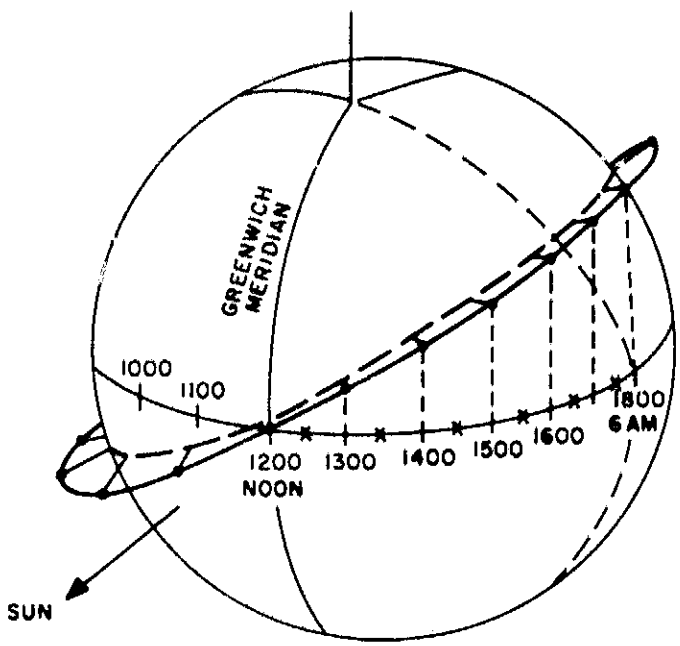

Figure 1. Simulated ASTP orbit geometry.

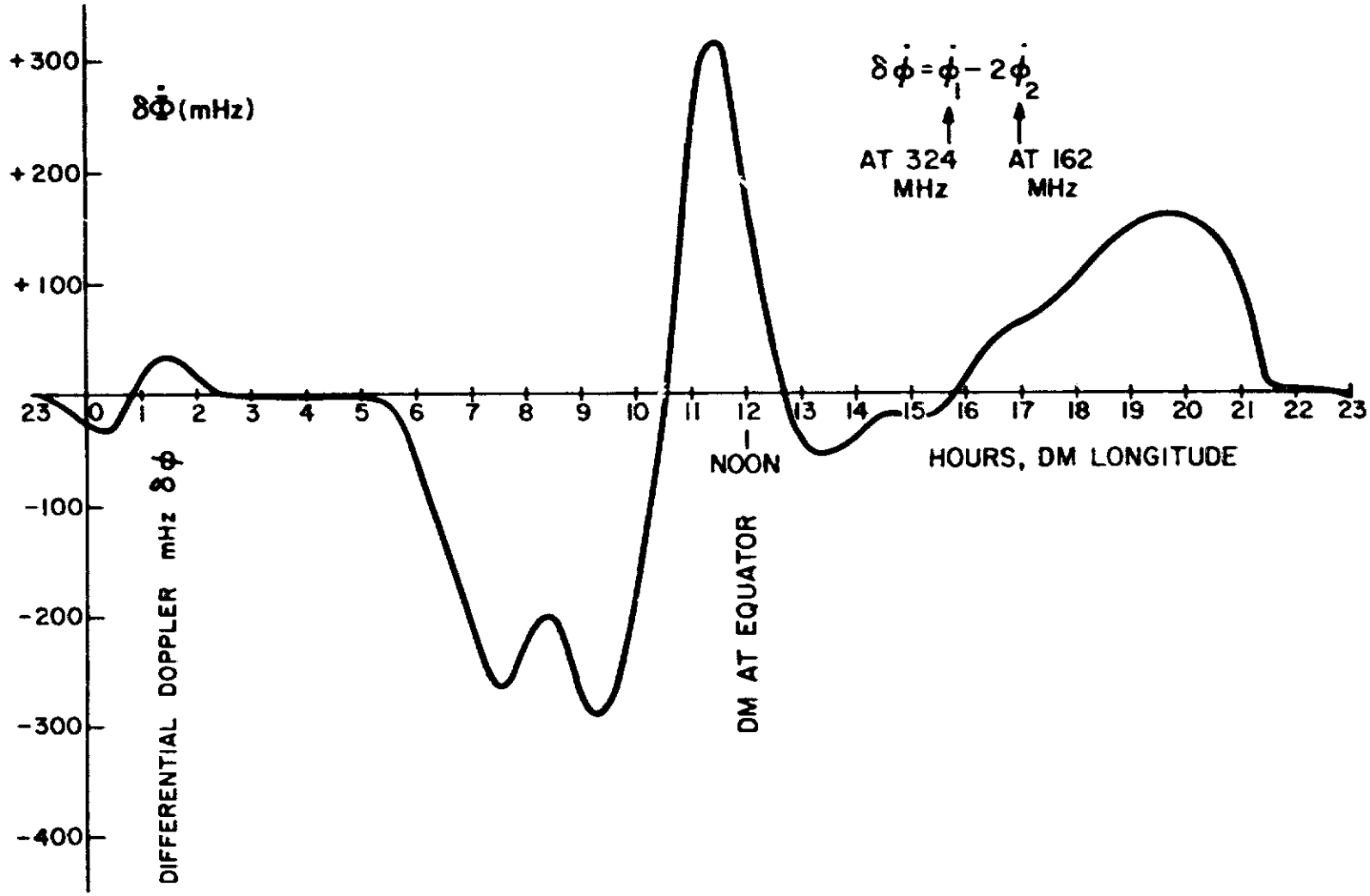

Figure 2. Expected differential doppler shift in the DM-to-CSM path for an entire orbit.

peak of about 300 to 400 mHz in $\delta\dot{\Phi}$, in contrast to the 2400 to 0500 LT region, where $\delta\dot{\Phi}$ is almost negligible. Overall, the horizontal gradients at the 221-km ASTP altitude vary by a factor of 100 between night and day.

In Figure 3, we show the horizontal gradient $\partial N/\partial\theta$ (in el cc^{-1} rad^{-1}) at the 221-km orbital height in the direction of increasing (eastward) orbital longitude θ. The solid curve is plotted through the averaged values $\Delta N/\Delta\theta$ at the midpoints of each 1-hour longitude interval (1230 LT, 1330 LT, ...). The broken curve is fitted to the expected average values measured by the DM/CSM link over the same 15° longitude intervals. Positive values indicate increasing electron density in the direction of orbital motion.

The extreme diurnal variation in $\overline{\partial N/\partial X}$ along the orbit could reflect on the gravitational part of the experiment, in that the maximum error of the ionospheric-related frequency shift in the individual frequencies varies from about 2 to 200%. Figure 4 indicates the allowable error in the determination of $\overline{\partial N/\partial\theta}$ as a function of gradient intensity for two values of maximum absolute error σ in the received frequency of the 324-MHz signal. For example, we see that for a value of $\overline{\partial N/\partial\theta} = 6 \times 10^5$ el cc^{-1} rad^{-1}, we must have less than a 2.2% error in the observed value of $\overline{\partial N/\partial X}$ (or $\overline{\partial N/\partial\theta}$) in order that the error in $\dot{\Phi}_1$ be less than 2 mHz. The nighttime region is the most attractive for detecting gravity anomalies, as least as far as the ionospheric effect is concerned. In daylight and transition regions (evening, morning), the required accuracy approaches 1% or less, suggesting that the likelihood of a small error in the ionospheric doppler correction masquerading as a gravity anomaly in the DM/CSM doppler record is greatly increased.

The preceding observation points out the absolute necessity of employing a phase-coherent dual-frequency link to measure the ionospheric frequency shift between spacecraft when accurate doppler range-rate measurements are desired. An a priori model of the ionosphere simply cannot be expected to embrace the evident accuracy requirements of the ASTP doppler-tracking experiment. To a high degree of accuracy, the individual corrections to the received frequencies f_1 and f_2 can be calculated from equations (3) and (4) to be

$$\dot{\Phi}_2 = \frac{f_1 f_2}{f_2^2 - f_1^2}\,\delta\dot{\Phi}$$

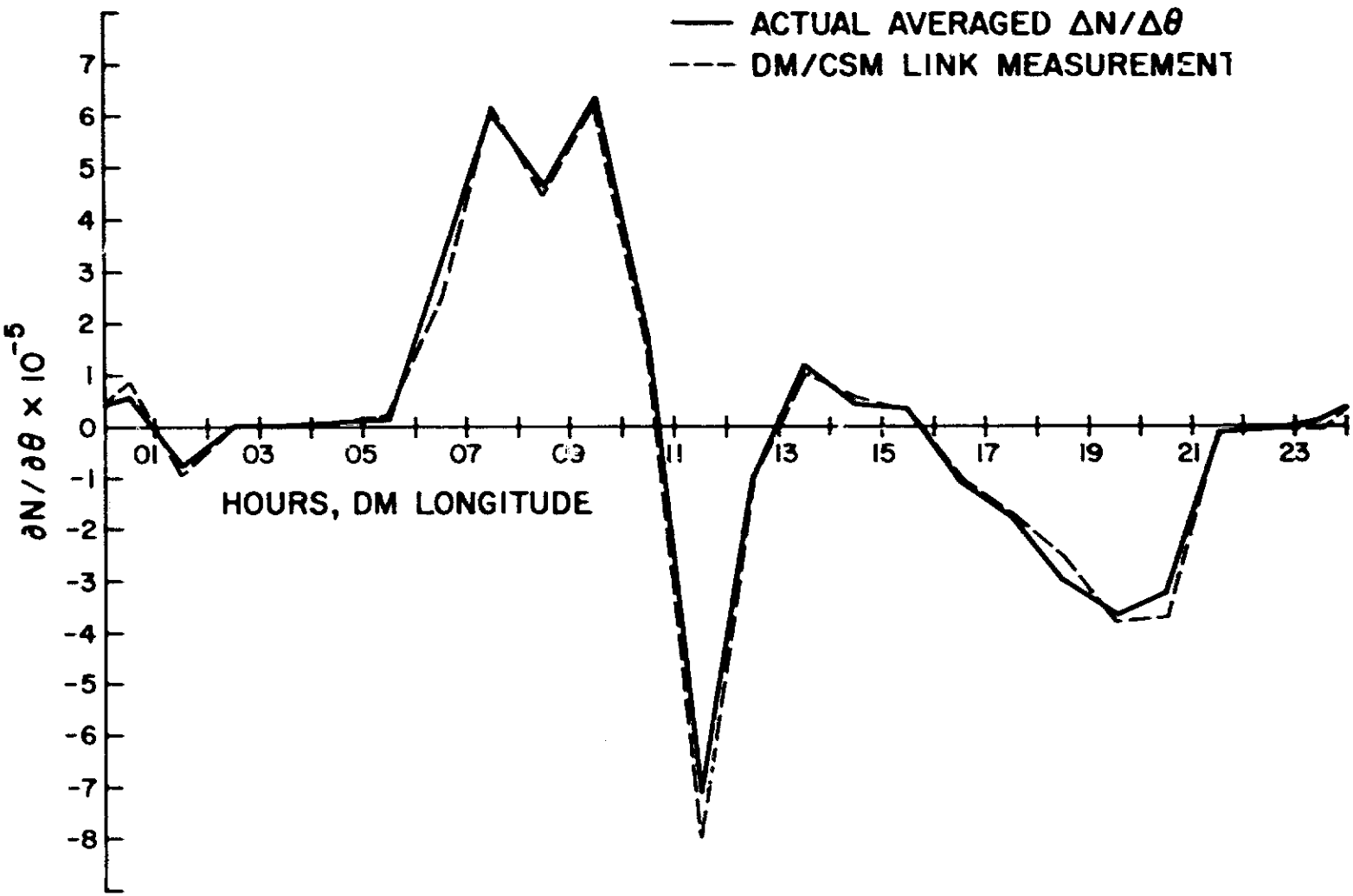

Figure 3. The horizontal electron-density gradient $\partial N/\partial\theta$, in el cc^{-1} rad^{-1}, at the 221-km orbital height.

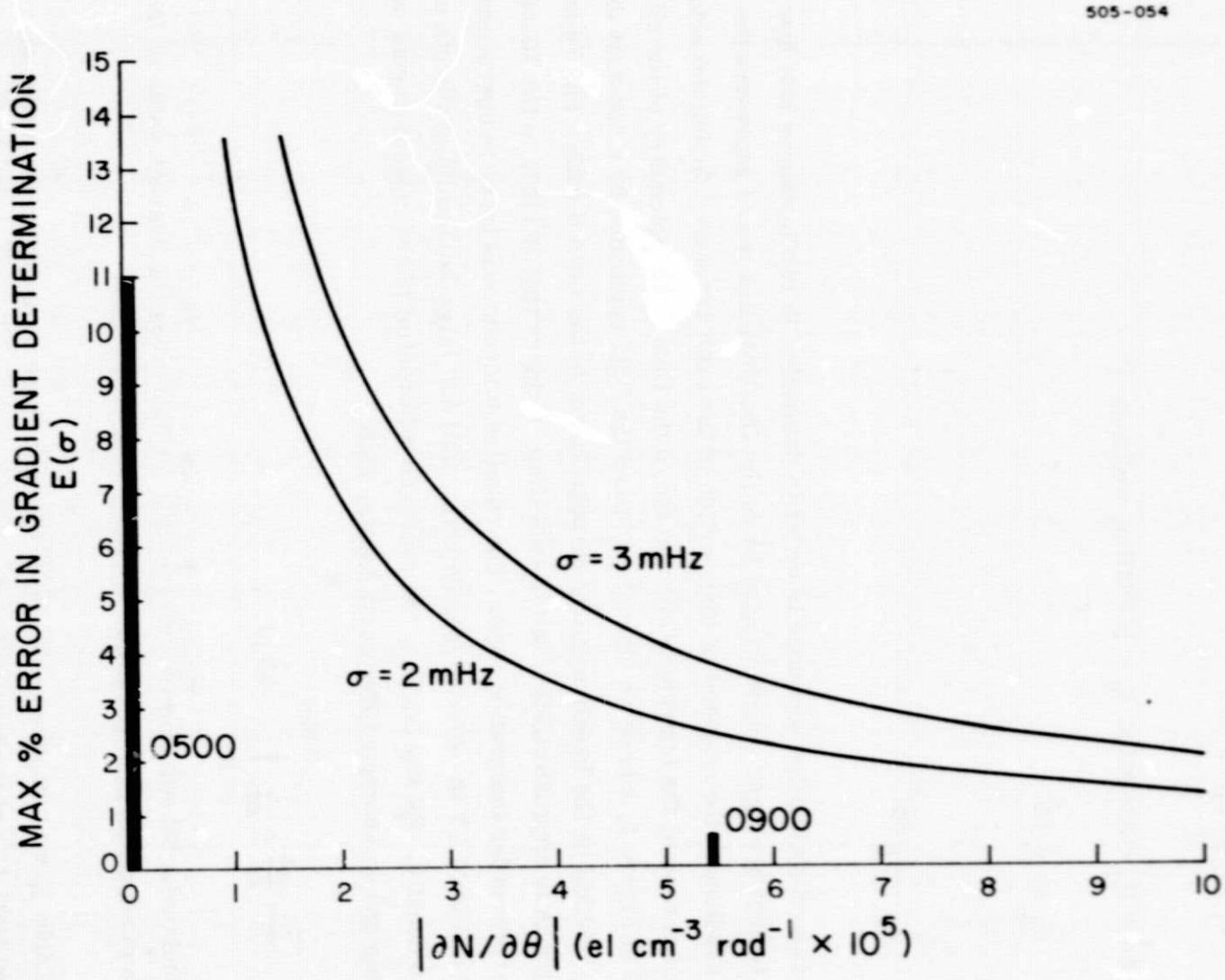

Figure 4. Error limits in determining the DM/CSM horizontal electron gradient at an altitude of 221 km.

and

$$\dot{\Phi}_1 = -\frac{f_2}{f_1}\dot{\Phi}_2 \quad .$$

In our case (f_1 = 324 MHz, f_2 = 162 MHz), we have

$$\dot{\Phi}_2 = -\frac{2}{3}\,\delta\dot{\Phi}$$

and

$$\dot{\Phi}_1 = -\frac{1}{3}\,\delta\dot{\Phi} \quad .$$

A second simulation was done in order to determine in two instances just how well a typical averaged observation of $\delta\dot{\Phi}$ in the DM/CSM link would represent the actual gradient at the midpoint of that portion of the orbit traversed during the actual integration time of the instrumentation on board the CSM. The geometry of the situation is seen in Figure 5, where we show the DM and the CSM separated by a constant distance of 300 km as the baseline moves through 70 km in the orbital path. The 70 km corresponds to approximately 9 sec of real time, a figure that is close to the 10-sec receiver/recorder integration time. The baseline midpoint was taken to correspond to 0500 and 0900 LT in order to include both small and large horizontal gradients of electron density. By ray tracing, the averaged differential phase measurements were simulated and an average differential doppler shift,

$$\overline{\delta\dot{\Phi}} = \frac{\Delta\Phi}{\Delta t} = \frac{1}{\Delta t}\int_0^{9\ \mathrm{sec}} \delta\dot{\Phi}\ dt \quad ,$$

was calculated. Substituting $\overline{\delta\dot{\Phi}}$ into equation (6) then gives the average value of $\partial N/\partial X$ over the moving DM/CSM baseline.

In Table 1, we compare values of $\overline{\partial N}/\partial X$ with those of $\partial N/\partial X$ at the midpoints (0500 and 0900 LT) of the moving baseline and note the associated relative error in $\overline{\partial N}/\partial X$. In both cases, the error is well below the maximum indicated in Figure 4. This is encouraging, but we must also consider the possible effects of time dependence

505-054

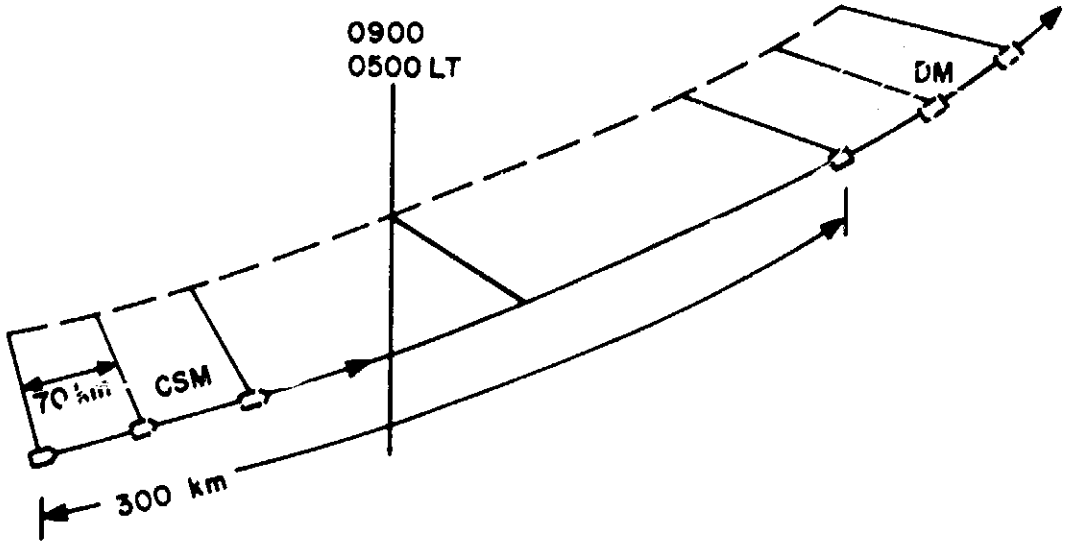

Figure 5. Geometry of individual 10-sec doppler-shift observations.

in the electron density ($\partial N/\partial t \neq 0$) and of large second-order derivatives $\partial^2 N/\partial X^2$, which would dislocate the mean point (where $\overline{\partial N}/\partial X = \partial N/\partial X$) from the assumed mid-point.

Table 1. DM/CSM gradient error.

Time	$\overline{\partial N}/\partial X$ (el cc^{-1} km^{-1})	$\partial N/\partial X$ (el cc^{-1} km^{-1})	Error in $\overline{\partial N}/\partial X$ (%)	Limit (%)
Night 0500 LT	16.5	14.9	11	136
Day 0900 LT	819	823	0.5	2.5

3. INVERSION OF SPACECRAFT-TO-GROUND DIFFERENTIAL AND ROTATING DOPPLER SHIFTS

3.1 Differential Doppler Shift

In this section, we will consider the various options available in analyzing spacecraft-to-ground differential doppler measurements. The effects of horizontal gradients and nonstationarity in the ionosphere complicate the problem considerably, but it is still possible to extract useful information about the ionosphere when measurements are made continually or at short intervals over a visible arc of the satellite orbit (Hibberd and Thomas, 1959; Al'pert et al., 1965; Tyagi, 1974). The effect of the ionosphere on spacecraft-to-ground doppler shifts is given precisely by the following relation:

$$\delta\dot{\Phi} = \frac{\omega_1}{c}\,\frac{2\pi e^2}{m}\left(\frac{1}{\omega_2^2} - \frac{1}{\omega_1^2}\right)\frac{d}{dt}\int_{\Gamma} N\, dS \quad . \tag{7}$$

Assumptions inherent in the above expression enter through equation (2).

Considering the electron density to be a function of coordinates and time,

$$N = N(x, y, z, t) \quad ,$$

leads to an expression involving those four quantities related to the differential doppler shift:

$$\delta\dot{\Phi} = \frac{\omega_1}{c}\,\frac{2\pi e^2}{m}\left(\frac{1}{\omega_2^2} - \frac{1}{\omega_1^2}\right)\left\{- N_c\,\frac{\dot{z}_c}{\cos\phi_c} + \left([\tilde{N}_R] + \left[\frac{\partial\tilde{N}}{\partial x}\right]\right)\left(\dot{r}_c + \frac{\dot{z}_c}{\cos\phi_c}\right) - \left[\frac{\partial\tilde{N}}{\partial y}\right]\dot{y}_c - \int\frac{\partial N}{\partial t}\,dS\right\} \quad , \tag{8}$$

following the notation of Al'pert (1965). In this equation, the satellite-borne transmitter is assumed to be moving with respect to an earth-fixed observing station through

a nonhomogeneous ionosphere, where the electron density at any point along the ray path may vary with time. The cartesian coordinates (x, y, z) of a point on the ray trajectory are given in an earth-fixed system centered at the ground station. The (x, z) plane contains the station, the instantaneous satellite position, and the center of the earth. The angle ϕ refers to the zenith angle of the ray trajectory, and the subscript c denotes values at the satellite position (x_c, y_c, z_c). In Figures 6a and 6b, the relationship between the various quantities can be more easily visualized. It is important to note that in the polar-coordinate system shown, the distance Rθ (or RX) from the origin is always positive, as is the zenith angle ϕ. As a consequence, directional derivatives of electron density $\partial N/\partial\theta$ and $\partial N/\partial X$ change discontinuously at the pole ($\phi_0 = 0$).

The first term within brackets in equation (8) relates the electron density in the vicinity of the satellite to the vertical velocity component $\dot{z}_c$ and is especially important in near-vertical rocket flights, where the vertical profile of N(z) can be easily mapped through observations of $\delta\dot{\Phi}$. The second term forms the contribution of the motion in the (R, θ) plane and defines the refraction angle $\delta\phi_0$ at the observing station. The term $-[\partial\tilde{N}/\partial y]\,\dot{y}_c$ gives the effect of motion normal to the (R, θ) plane and defines the corresponding transverse refraction angle $\delta\psi_0$. The final term, $-\int \partial N/\partial t\, dS$, accounts for the fact that the electron density along the ray path may be changing independently with time. Normally, it is quite small (Al'pert, 1965) compared to the other terms and can be neglected unless a large-scale ionospheric disturbance occurs in the spacecraft-to-ground path.

The integrals $[\tilde{N}_R]$ and $[\partial\tilde{N}/\partial x]$ are taken along the ray path Γ, which, to first order, can be considered to coincide with the geometric line of sight. They represent the mean electron density and the mean horizontal gradient in electron density between the satellite and the ground station. In terms of spherical coordinates, these quantities are expressed as follows (R_0 = earth's radius):

$$[\tilde{N}_R] = \frac{\int NR\,(R\cos\phi)^{-3}\,dR}{(R_0\cos\phi_0)^{-1} - (R_c\cos\phi_c)^{-1}}\quad , \tag{9}$$

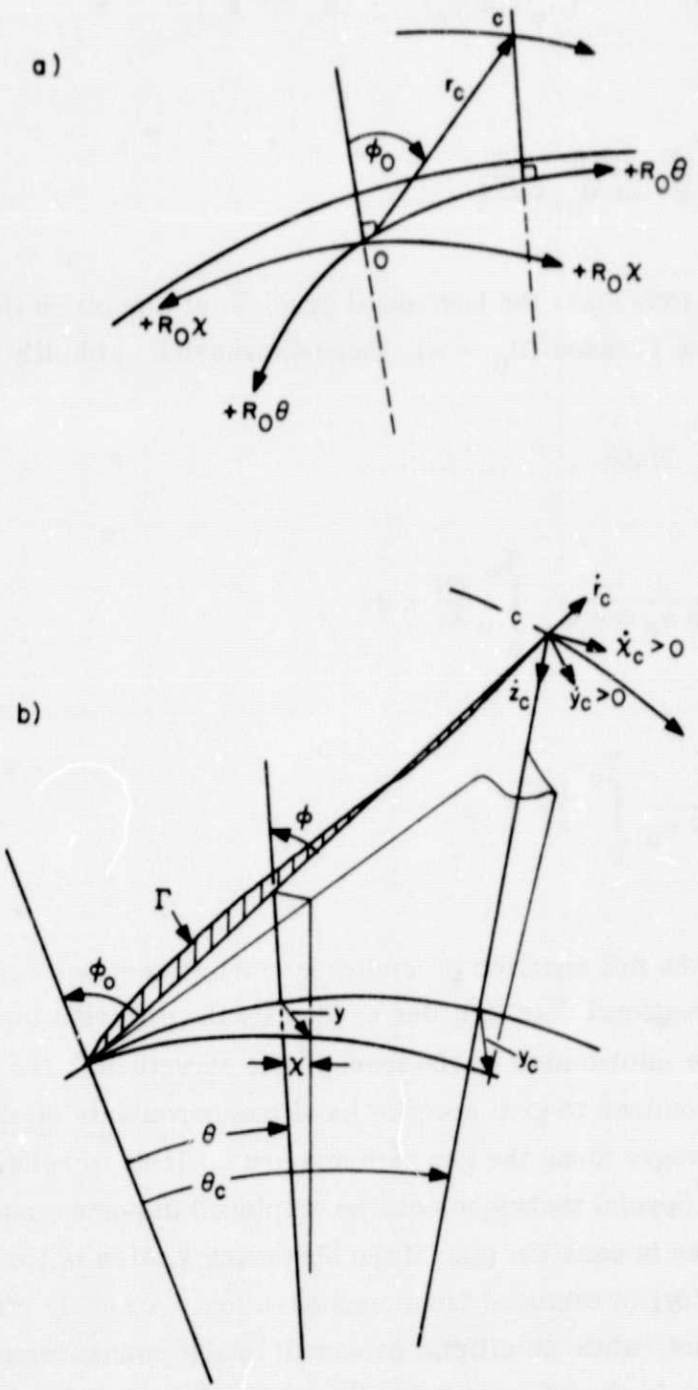

Figure 6. a) Ground-station polar coordinates. b) Geometry of spacecraft-to-ground ray path.

$$\left[\frac{\partial \tilde{N}}{\partial x}\right] = \frac{1}{\sin \phi_0} \int \frac{\partial N}{\partial x} \frac{(R_0 \cos \phi_0)^{-1} - (R \cos \phi)^{-1}}{(R_0 \cos \phi_0)^{-1} - (R_c \cos \phi_c)^{-1}} \frac{dR}{\cos \phi} \quad , \tag{10}$$

and

$$\left[\frac{\partial \tilde{N}}{\partial y}\right] = \frac{R_0}{R_c} \int \frac{\partial N}{\partial y} \frac{\sin \theta}{\sin \theta_c} \frac{dR}{\cos \phi} \quad , \tag{11}$$

where $\partial N/\partial X = (1/R)\,(\partial N/\partial \theta)$ is the horizontal gradient at a point on the ray path. If a planar approximation is made ($R_0 \to \infty$), these expressions simplify to

$$[\tilde{N}_R] = \frac{1}{z_c} \int_0^{z_c} N \, dz \quad , \tag{9a}$$

$$\left[\frac{\partial \tilde{N}}{\partial x}\right] = \frac{1}{z_c \sin \phi_0 \cos \phi_0} \int_0^{z_c} \frac{\partial N}{\partial x} \, z \, dz \quad , \tag{10a}$$

and

$$\left[\frac{\partial \tilde{N}}{\partial y}\right] = \frac{1}{z_c \cos \phi_0} \int_0^{z_c} \frac{\partial N}{\partial y} \, z \, dz \quad . \tag{11a}$$

The inversion of the full equation (8) embraces many questions concerning just how to treat the observational data in order to identify the different terms and obtain from them any definite information on the ionospheric structure. The local term N_c is the only one that promises to give specific local measurements of electron density; all the others are averages along the ray path and are difficult to relate to particular ionospheric regions. Special techniques can be employed in some cases to reduce the number of unknowns in equation (8). If the observing station is located in the plane of the orbit, then $[\partial N/\partial y]$ is removed from consideration. A nearly circular orbit renders N_c insignificant, while an elliptic orbit will enable measurements to be made when $\dot{r}_c + (\dot{z}_c/\cos \phi_0) = 0$, thereby removing $[\tilde{N}_R]$ and $[\partial \tilde{N}/\partial x]$. This last condition has been exploited by Al'pert and Sinel'nikov (1965) to measure $[\partial \tilde{N}/\partial y]$ and N_c.

3.2 Rotating Doppler Shift

The rotating doppler (or Faraday rotation) effect can also be used to obtain electron-density information if a linearly polarized antenna is utilized at the observing station. The frequency of amplitude variation of the circularly polarized wave as received is given by Al'pert (1965), where quasi-longitudinal propagation and a constant magnetic-field vector along the ray path are assumed. The rotating doppler shift is then given by

$$\dot{\phi}_H = \mp \frac{2\pi e^2}{m\omega^2} \frac{\omega_H}{c} \left\{ - N_c \dot{z}_c \frac{\cos \Theta_c}{\cos \phi_c} + \left([\tilde{N}_{RH}]_1 + \left[\frac{\partial \tilde{N}}{\partial x}\right]_H \right) \left(\dot{r}_c + \frac{\dot{z}_c}{\cos \phi_c} \right) \right.$$

$$\left. - \left([\tilde{N}_{RH}]_2 - \left[\frac{\partial \tilde{N}}{\partial y}\right]_H \right) \dot{y}_c - \left[\frac{\partial \tilde{N}}{\partial t}\right]_H \right\} . \qquad (12)$$

Here, the minus and plus signs refer to the ordinary and extraordinary waves, respectively, and the signs of $\dot{r}_c$, $\dot{z}_c$, and $\dot{y}_c$ are determined in the same way as in the differential doppler shift. The quantities in brackets are

$$[\tilde{N}_{RH}]_1 = \frac{\sin \gamma_0 \cos \xi_0}{R_0 \sin \phi_0 \left[(R_0 \cos \phi_0)^{-1} - (R_c \cos \phi_c)^{-1} \right]} \int \frac{N R^2 \, dR}{(R \cos \phi)^3} , \qquad (13)$$

$$\left[\frac{\partial \tilde{N}}{\partial x}\right]_H = \frac{1}{\sin \phi_0} \int \frac{\partial N}{\partial x} \frac{\cos \Theta}{\cos \phi} \frac{(R_0 \cos \phi_0)^{-1} - (R \cos \phi)^{-1}}{(R_0 \cos \phi_0)^{-1} - (R_c \cos \phi_c)^{-1}} \, dR , \qquad (14)$$

$$[\tilde{N}_{RH}]_2 = \pm \frac{\sin \gamma_0 \sin \phi_0 \sin \xi_0}{\theta_c} \int \frac{N \, dR}{R \cos \phi} , \qquad (15)$$

$$\left[\frac{\partial \tilde{N}}{\partial y}\right]_H = \frac{R_0}{R_c} \int \frac{\partial N}{\partial y} \frac{\sin \theta}{\sin \theta_c} \frac{\cos \Theta}{\cos \phi} \, dR , \qquad (16)$$

and

$$\left[\frac{\partial \tilde{N}}{\partial t}\right]_H = \int \frac{\partial N}{\partial t} \frac{\cos \Theta}{\cos \phi} \, dR . \qquad (17)$$

The following quantities are depicted in Figure 7:

$\vec{H}_0$ = the magnetic-field vector,

Θ = the angle between the magnetic-field vector and the wave normal,

γ_0 = the angle between the magnetic-field vector and the geocentric radius vector,

ξ_0 = the angle between the geometric ray of sight and the projection of $\vec{H}_0$ onto the local horizontal plane.

The upper sign in equation (15) is used when $d\xi_0/dt > 0$, or when the projection of $\vec{H}_0$ on the local horizontal plane is moving away from the (R, θ) plane.

As in the differential doppler relations, a planar approximation clarifies the relationships between the quantities in equations (13) to (17) and the physical ionospheric parameters. In the flat-earth case, equations (13) to (17) become

$$[\tilde{N}_{RH}]_1 = \frac{\sin \gamma_0 \cos \xi_0}{z_c \sin \phi_0} \int_0^{z_c} N \, dz \quad , \tag{13a}$$

$$\left[\frac{\partial \tilde{N}}{\partial x}\right]_H = \frac{\cos \Theta_0}{z_c \sin \phi_0 \cos \phi_0} \int_0^{z_c} \frac{\partial N}{\partial x} z \, dz \quad , \tag{14a}$$

$$[\tilde{N}_{RH}]_2 = \pm \frac{\sin \gamma_0 \sin \xi_0}{z_c} \int_0^{z_c} N \, dz \quad , \tag{15a}$$

$$\left[\frac{\partial \tilde{N}}{\partial y}\right]_H = \frac{\cos \Theta_0}{z_c \cos \phi_0} \int_0^{z_c} \frac{\partial N}{\partial y} z \, dz \quad , \tag{16a}$$

and

$$\left[\frac{\partial \tilde{N}}{\partial t}\right]_H = \frac{\cos \Theta_0}{\cos \phi_0} \int_0^{z_c} \frac{\partial N}{\partial t} \, dz \quad , \tag{17a}$$

where $R_0 \to \infty$, $dR \to dz$, and the angles ϕ and Θ are constant.

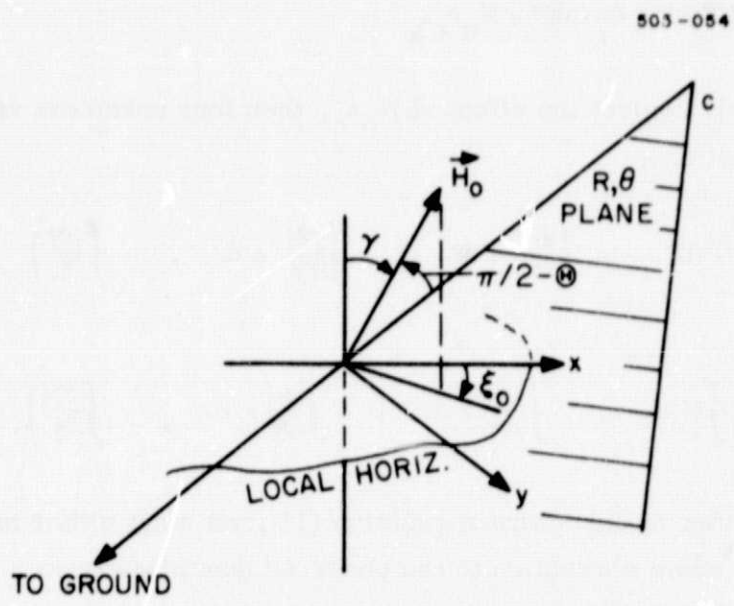

Figure 7. Geometry and notation of rotating doppler shift.

In the absence of horizontal gradients, we have $\delta\dot{\Phi}_H$ for the two frequencies and a differential doppler shift, $\delta\dot{\Phi}$, which can be used to solve for $\int N\,dz$ and N_c for each point observed during a pass. The value of N_c will be less significant because of the near circularity of the satellite (DM) orbit. For the ASTP mission, the planned eccentricity of 0.0002 during the doppler tracking phase results in an amplitude of approximately 1.5 m sec^{-1} in $\dot{z}_c$. Assuming $N_c = 10^6$ el cc^{-1}, this value of $\dot{z}_c$ would contribute at most about 2 mHz to the received differential doppler shift. This is a negligible value, but an increase in a few kilometers in the apogee/perigee height difference could combine with an electron density of several times 10^6 el cc^{-1} to give a nonnegligible value of perhaps 20 mHz owing to $N_c\dot{z}_c$.

If we can safely neglect the effect of $N_c\dot{z}_c$, then four unknowns remain in the system of two equations:

$$\delta\dot{\Phi} = f\left(\int N\,dz \;,\; \int\frac{\partial N}{\partial x}\,z\,dz \;,\; \int\frac{\partial N}{\partial y}\,z\,dz \;,\; \int\frac{\partial N}{\partial t}\right) \;,$$

$$\delta\dot{\Phi}_H = g\left(\int N\,dz \;,\; \int\frac{\partial N}{\partial x}\,z\,dz \;,\; \int\frac{\partial N}{\partial y}\,z\,dz \;,\; \int\frac{\partial N}{\partial t}\right) \;. \qquad (18)$$

To reduce the number of unknowns in equation (18), we must either neglect the gradient integrals or make some correction to the observed quantities from a priori knowledge of $\partial N/\partial x$ and $\partial N/\partial y$ along the ray paths. Another condition that can be met for at least one observing station is that the effect of $\int(\partial N/\partial y)\,z\,dz$ can be made small in comparison to the remaining terms by locating the receiver near the orbital plane. Then, if $\partial N/\partial t$ can be accounted for, the system (18) is not insoluble.

4. THE INFLUENCE OF HORIZONTAL GRADIENTS ON THE SPACECRAFT-TO-GROUND DATA-INVERSION ACCURACY

4.1 Inversion in the Presence of Unknown Horizontal Gradients

If the gradient-related terms $[\partial\tilde{N}/\partial x]$ and $[\partial\tilde{N}/\partial y]$ are neglected and the time stationarity of the electron density N is assumed, then we can assign the total $\delta\dot{\Phi}$ to the effect of the path's average electron density $[\tilde{N}_R]$. Equation (8) then becomes

$$\delta\dot{\Phi} = a_0 \left(\dot{r}_c + \frac{\dot{z}_c}{\cos \phi_0} \right) \frac{1}{z_c} \int_0^{z_c} N(x, z)\, dz \tag{19}$$

with the planar approximation in effect. We note here that the integral $(1/z_c) \int N\, dz$ is closely approximated by the average electron density along the straight-line path connecting the receiver with the transmitter, $(1/\rho_c) \int_0^{\rho_c} N(x, z)\, d\rho$, and we will use these interchangeably. Since the gradient term $[\partial\tilde{N}/\partial x]$ can be either negative or positive, depending on the geometry of the situation, we can accordingly expect the estimate of $[\tilde{N}_R]$ to be too large or too small. However, we do not expect that gradients large enough to change the sign of $\delta\dot{\Phi}$ would exist along the spacecraft-to-ground path except when the satellite is almost exactly above the observing station. The inversion of $\delta\dot{\Phi}$ to columnar electron content by means of equation (19) suffers especially near the point where $\phi_0 = 0$. This is easily seen by considering the equation

$$\delta\dot{\Phi} = a_0 \left[\left(\dot{r}_c + \frac{\dot{z}_c}{\cos \phi_0} \right) \frac{1}{z_c} \int_0^{z_c} N\, dz + \left(\dot{r}_c + \frac{\dot{z}_c}{\cos \phi_0} \right) \frac{1}{z_c \cos \phi_0 \sin \phi_0} \int_0^{z_c} \frac{\partial N}{\partial x}\, z\, dz \right] . \tag{20}$$

If the orbit is circular, then the expression for $(1/z_c) \int N\, dz$ in terms of $\delta\dot{\Phi}$ is

$$\frac{1}{z_c} \int N\, dz = \frac{\delta\dot{\Phi}}{a_0 \dot{x}_c \sin \phi_0} - \frac{1}{z_c \sin \phi_0 \cos \phi_0} \int \frac{\partial N}{\partial x}\, z\, dz \quad . \tag{21}$$

Ideally, in the absence of gradients, $\delta\dot{\Phi} \to 0$ as $\phi_0 \to 0$, and it is possible to calculate $\int N\, dS$ near the vertical by numerical application of the l'Hospital rule. In reality, however, we obtain the value

$$[\tilde{N}_R] + \left[\frac{\partial \tilde{N}}{\partial x}\right] = \frac{\delta\dot{\Phi}}{a_0 \dot{x}_c \sin \phi_0} \quad , \tag{22}$$

which may include a sizable horizontal-gradient effect. When the satellite is directly over the station ($\phi_0 = 0$), the differential doppler shift will be approximately

$$\delta\dot{\Phi}_0 = \frac{a_0 \dot{x}_c}{z_c \cos \phi_0} \int_0^{z_c} \frac{\partial N}{\partial x}\, z\, dz \quad , \tag{23}$$

or simply a function of the horizontal gradient. Again, this is an idealization, since the higher order effects neglected in deriving the above equations will at times add a few percent to the theoretical value of $\delta\dot{\Phi}$. One example is that of the overhead ($\phi_0 = 0$) case. The doppler shift of each frequency depends not on the straight-line relative velocity between the antenna centers but on the component in the direction of the wave normal at the emitter (Al'pert, 1963). The difference becomes important near the vertical and will be manifested as a small displacement from the vertical of the direction where $\delta\dot{\Phi} = 0$. We mention these effects primarily because of their importance in the idealized simulation of $\delta\dot{\Phi}$ and in the subsequent recovery of ionospheric parameters. The actual observations will have components due to out-of-plane motion, orbital eccentricity, and nonstationarity of the ionosphere ($\partial N/\partial t \neq 0$) predominating over the small second-order omissions in the theory.

In order to demonstrate what we can expect in the actual data reduction, we have simulated the DM-to-ground differential doppler records for three widely varying ionospheric conditions. Equation (8) is simplified by a circular orbit of the satellite ($\dot{z}_c = 0$) with the ground station always in the orbital plane ($\dot{y}_c = 0$). Furthermore, the effect of nonstationarity [$\partial N/\partial t$] is excluded. For the simulation, we chose to locate the ground station at positions corresponding to 0430, 0930, and 1230 LT. At 0430 LT, the electron density is lowest, with correspondingly small gradients, and is the least interesting case for our purposes. The small doppler shifts simulated are

subject to a larger relative measurement error, and computer time limitations on the ray-tracing accuracy prevented us from making any clear distinction of the small gradient effects. We will therefore concentrate on the 0930 and 1230 LT cases, where the horizontal gradients are clearly significant.

One way to examine the effect of neglecting $\partial N/\partial x$ in the inversion is to compare the total simulated $\delta\dot{\Phi}$ with the theoretical value, given by

$$\delta\dot{\Phi}_c = a_0 \left(\dot{r}_c + \frac{\dot{z}_c}{\cos \phi_0} \right) \frac{1}{\rho_c} \int_0^{\rho_c} N \, dS \quad , \tag{24}$$

where the integral is computed directly from the ionospheric model. We shall call $\delta\dot{\Phi}_c$ the "columnar" doppler shift, to denote its dependence only on the average columnar electron content between the satellite and the ground station. Figures 8a, 8b, and 8c show the relationship between $\delta\dot{\Phi}$ and $\delta\dot{\Phi}_c$ for various elevation angles with the station at 0430, 0930, and 1230 LT. The elevation E is measured positively from the horizon over which the satellite approaches the station.

The inversion of our expected $\delta\dot{\Phi}$ to columnar electron content without accounting in any way for the $[\partial\tilde{N}/\partial x]$ term is perilous indeed. In Figure 9a, we have plotted the expected actual columnar electron content for the 1230 LT DM-to-ground case (curve A), and it should be compared with curve B, which gives the columnar electron content obtained by simply inverting equation (19) for $\int N \, dS$. There is a sizable error throughout the pass and a noticeable divergence near the vertical, owing to the fact that $\delta\dot{\Phi}$ approaches not zero, but the value given by equation (23). By applying the l'Hospital rule at $\phi_0 = 0$, we get a value of $[\tilde{N}_R]_0 + [\partial\tilde{N}/\partial x]_0$; the corresponding apparent columnar electron content is identified by B_L in Figure 9a.

At 0930 LT, the horizontal gradient is much larger, as evidenced by the value at 221 km (Figure 3), and the effect on curve B (Figure 9b) is severe.

An immediate correction can be introduced by assuming $\int (\partial N/\partial x)\, z \, dz$ to be constant throughout the satellite pass if $\delta\dot{\Phi}_0 = \delta\dot{\Phi}(\phi_0 = 0)$ can be detected. Within the first-order planar-approximation theory,

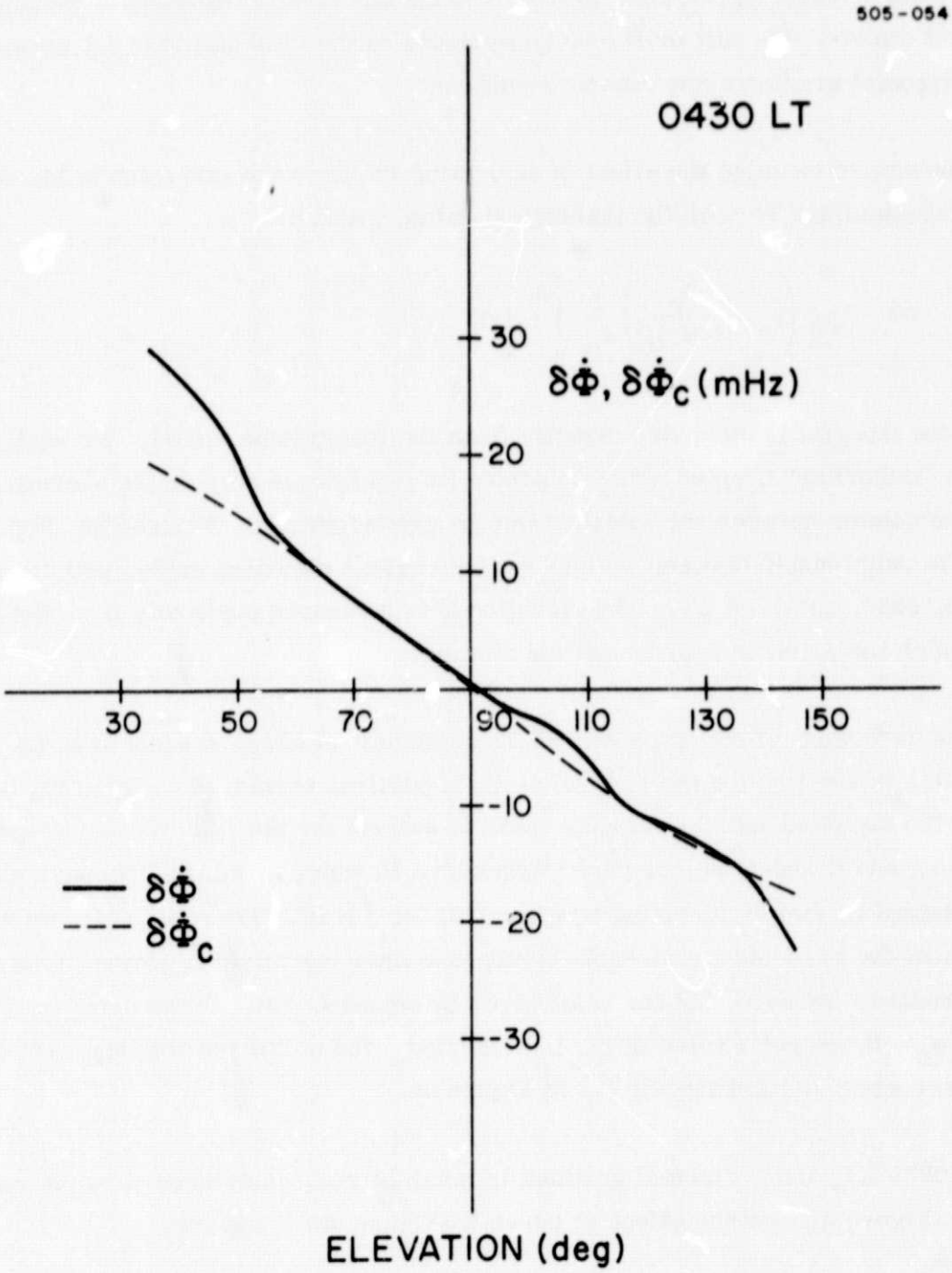

Figure 8a. Expected differential doppler shift in the DM-to-ground path at 0430 LT.

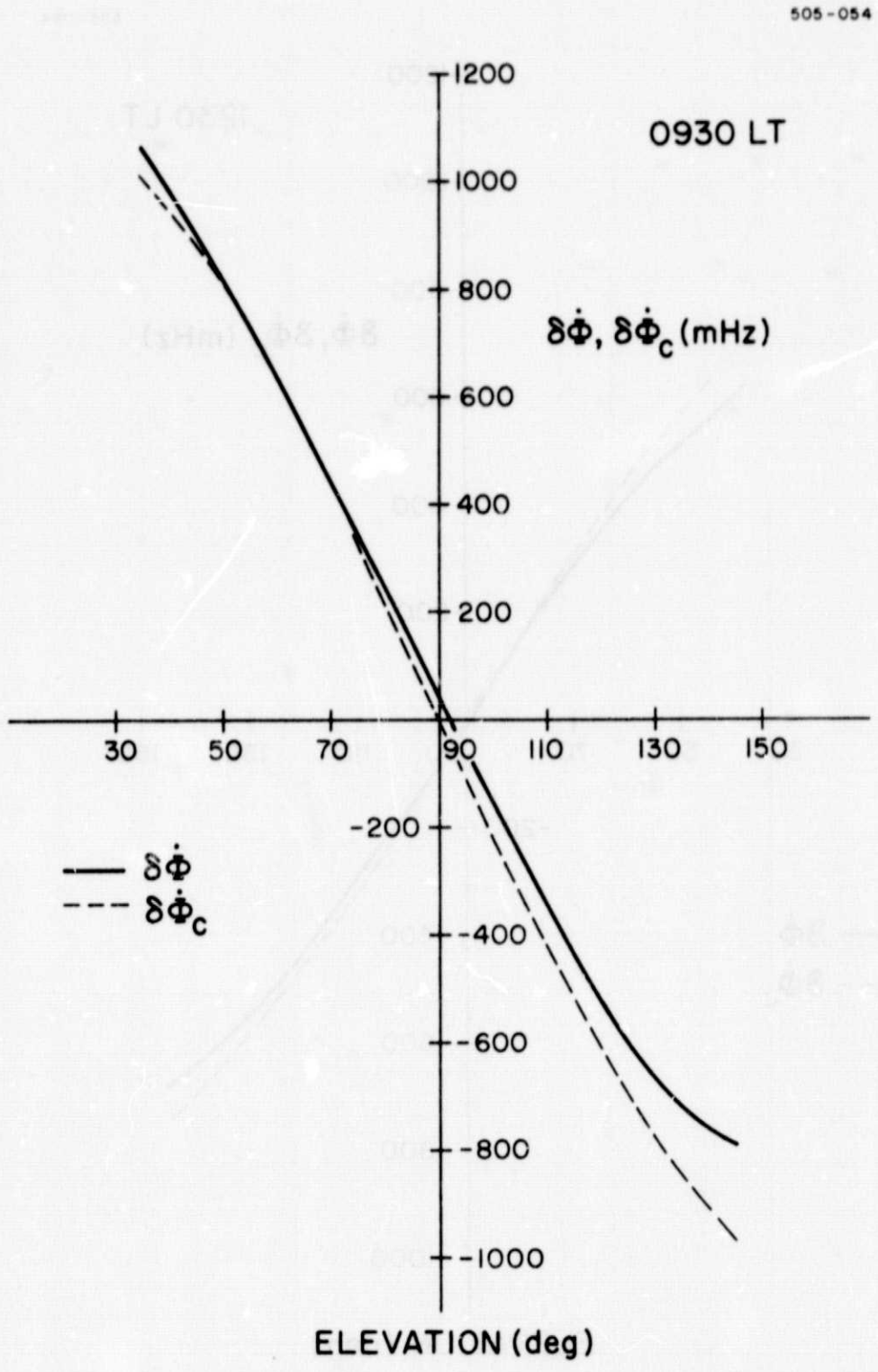

Figure 8b. Expected differential doppler shift in the DM-to-ground path at 0930 LT.

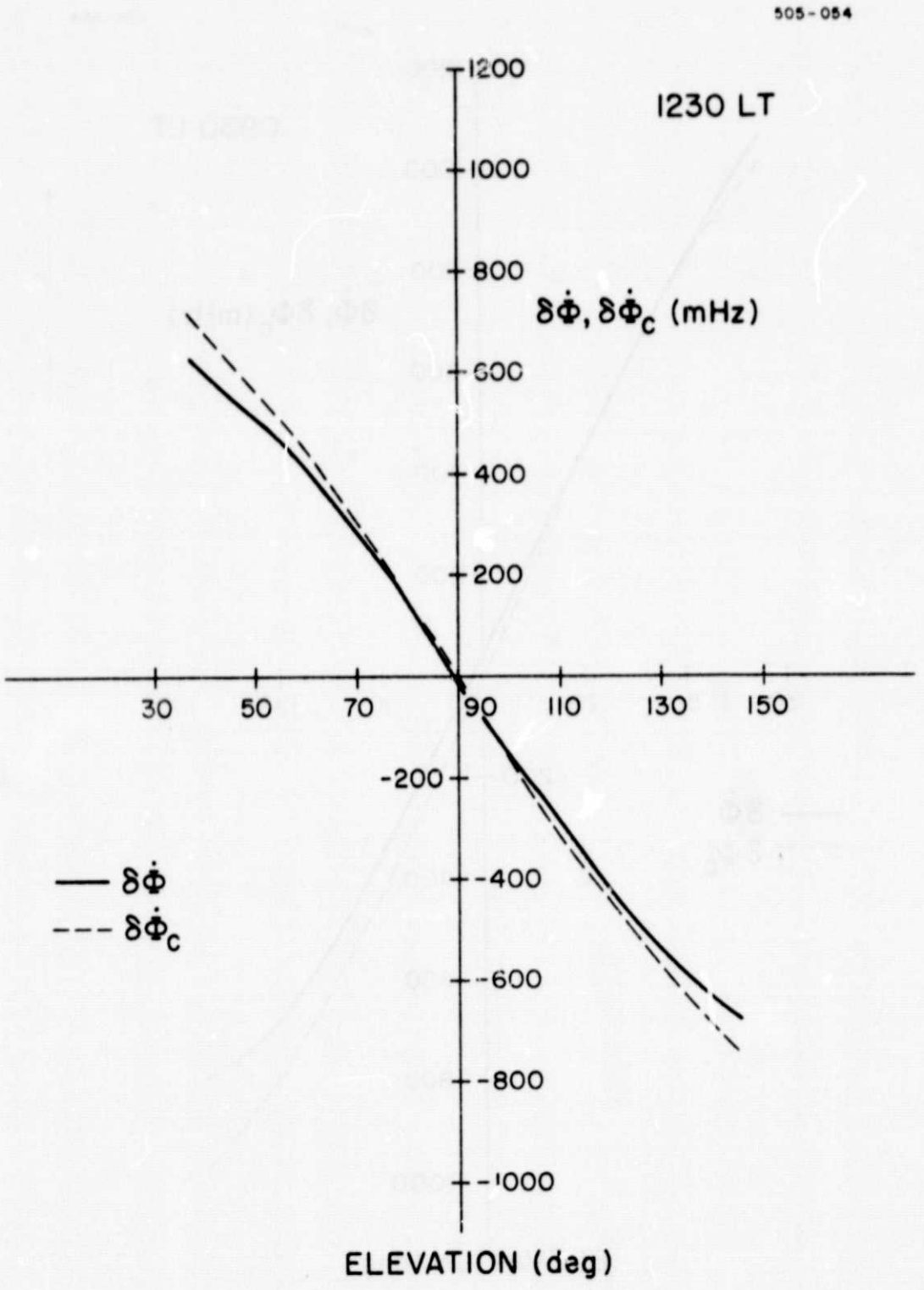

Figure 8c. Expected differential doppler shift in the DM-to-ground path at 1230 LT.

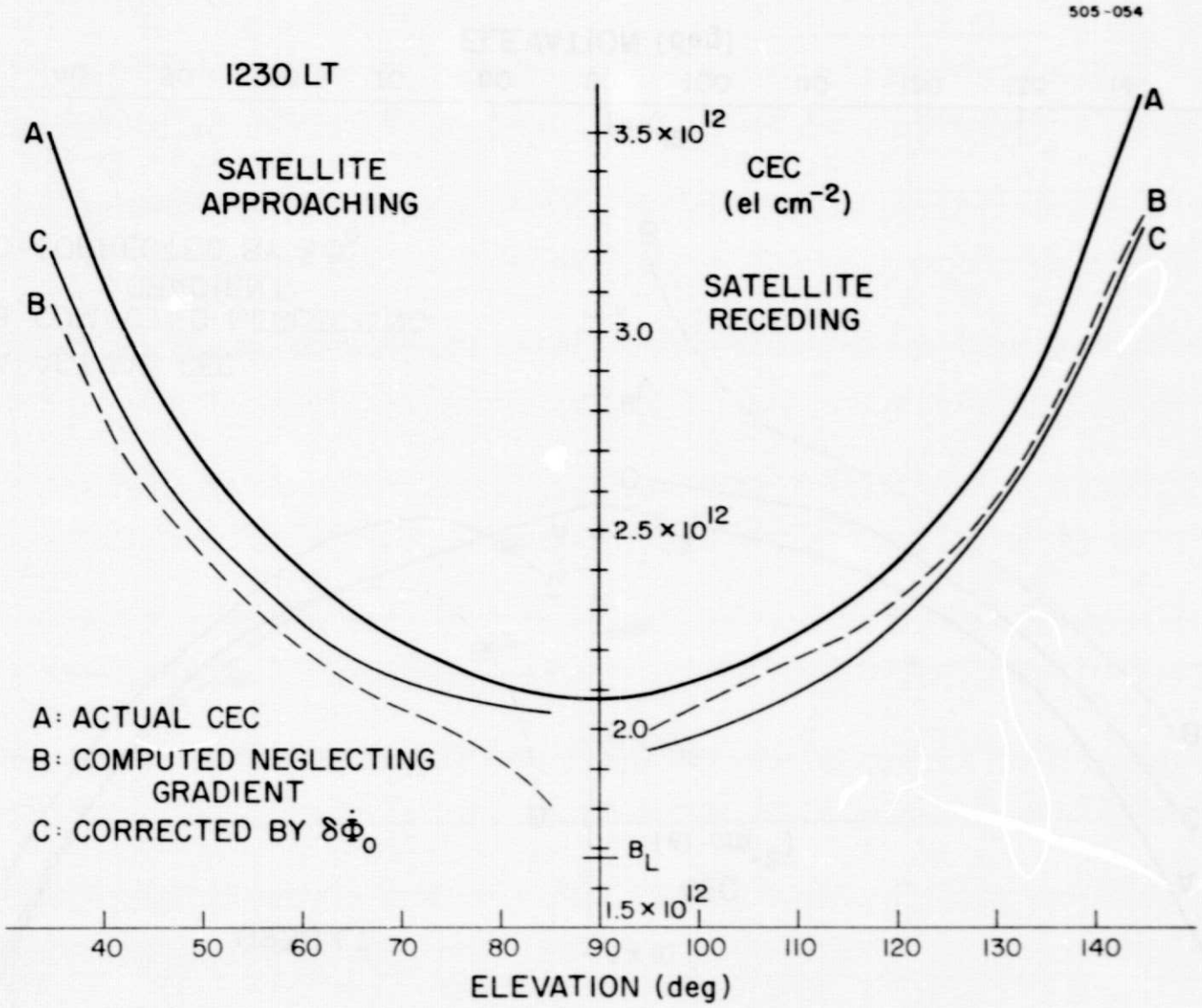

Figure 9a. Columnar electron content (CEC) in the DM-to-ground path at 1230 LT.

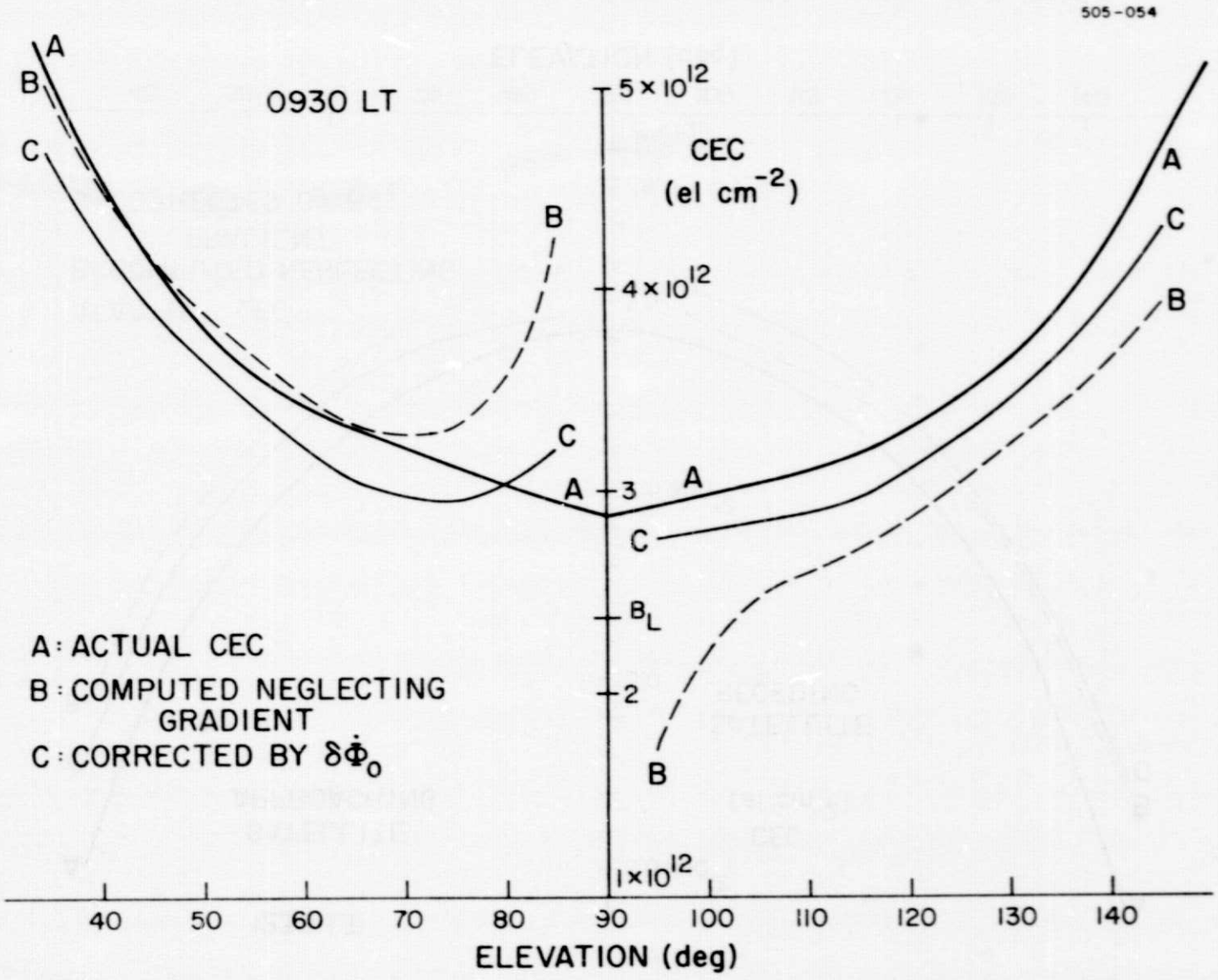

Figure 9b. Columnar electron content in the DM-to-ground path at 0930 LT.

$$\delta\dot{\Phi}_0 = a_0 \dot{x}_c \int_0^{z_c} \frac{\partial N}{\partial x} z \, dz \quad . \tag{25}$$

If the integral in equation (25) is a function of z_c only, then its contribution to $\delta\dot{\Phi}$ is simply $\delta\dot{\Phi}_0/\cos\phi_0$, which can be subtracted before solving for the columnar electron content. By interpolation about $\phi_0 = 0$, we found a value of $\delta\dot{\Phi}_0 = +38$ mHz for the 0930 LT pass and a smaller negative value of -8.7 mHz for 1230 LT. Applying equation (25) and using the integral calculated from our model ionosphere (Grossi and Gay, 1975, Appendix A), we found the corresponding theoretical values of $\delta\dot{\Phi}_0$ to be -7 and +39.3 mHz. Hence, if the $\delta\dot{\Phi}$ record is sufficiently smoothed near $\phi_0 = 0$, we can obtain $\delta\dot{\Phi}(0)$ rather accurately in the presence of a large horizontal gradient. The corrected columnar electron content is represented by curve C in Figures 9a and 9b. This correction succeeds in removing a large part of the error near $\phi_0 = 0$, but it is less effective at larger angles since it does not take into account the longitudinal variation of $\int(\partial N/\partial x)\, z\, dz$, an effect that can be seen at 0930 LT, where the gradient contribution on the left ($E < 90°$) is much smaller than that on the right. Hence, curve C reflects an overcorrection to the columnar electron content on the left-hand side. In Figure 9a, the correction is actually in the wrong direction for $E > 90°$ but reduces the error considerably on the left.

4.2 Inversion by Use of Simply Modeled Horizontal Gradients

A suitable ionospheric electron-density model incorporating knowledge of horizontal gradients can be employed to estimate the effects of $\partial N/\partial x$ and $\partial N/\partial y$ on the observed $\delta\dot{\Phi}$. The layer models of Chapman (1931) have a wide application in this type of procedure, and several variations can be considered. The selection of a particular model should be affected by the most current reliable observations and predictions of ionospheric electron density for the time of the ASTP mission.

In our simulation of data reduction, we have chosen the simplest of models, a linear variation of $\partial N/\partial x$ with altitude. Since the number of free electrons (and $\partial N/\partial x$) diminishes to nearly zero at heights of 70 to 80 km, we chose a linear profile, as depicted in Figure 10, where $\partial N/\partial x$ is zero below 70 km and takes the value of $(\partial N/\partial x)\big|_c$ given by the model used in the simulation (Grossi and Gay, 1975, Appendix A).

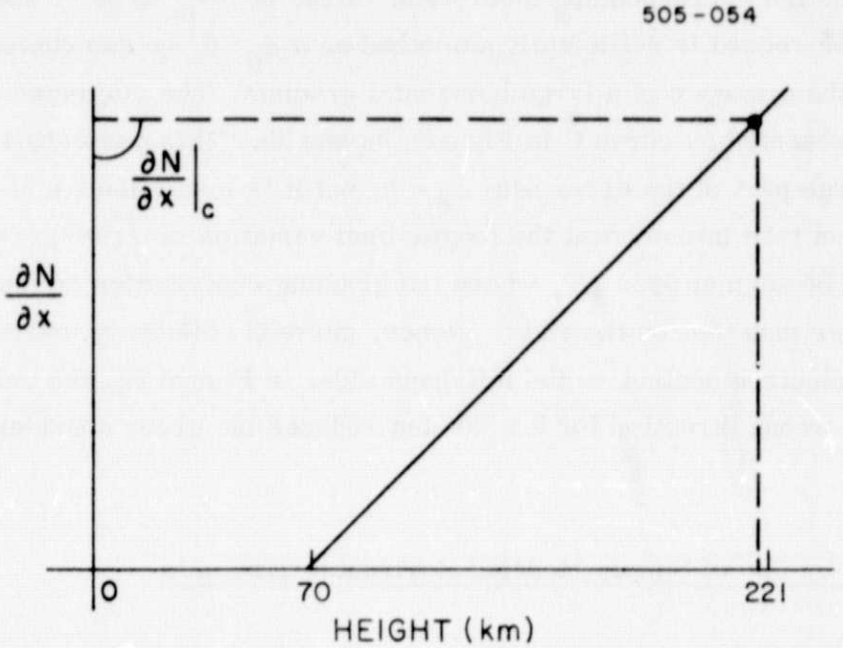

Figure 10. Linear gradient profile.

The results obtained by incorporating these linear-model gradients into the calculation of the total electron content are given in Figures 11a and 11b. The curves labeled D represent the columnar electron content obtained from $\delta\dot{\Phi}$ after corrections have been made for the effect of $[\partial\tilde{N}/\partial x]$ computed from the above model. In the 1230 LT case (Figure 11a), curve D would fall between curves B and C in both quadrants in Figure 9a. The correction based on the a priori linear model is then somewhat less effective than the correction applied by using $\delta\dot{\Phi}_0$.

At 0930 LT (Figure 11b), curve D if plotted in Figure 9b would fall below curve C during the satellite's approach to the ground station, and in the receding quadrant, it would fall between C and the actual columnar-electron-content curve (A). It is apparent that the change in $[\partial\tilde{N}/\partial x]$ with elevation during a pass is significant and that a more sophisticated model is needed.

4.3 Application of Spacecraft-to-Spacecraft Horizontal Gradient Measurements

Instead of relying completely on models of $\partial N/\partial x$, we are able, in the ASTP experiment, to utilize the actual measurements of the horizontal gradient in the DM/CSM path in the data reduction. It is well known that the ionosphere is not ideally smooth over the characteristic observing period of 2 to 3 min required for a satellite pass (Al'pert and Sinel'nikov, 1965). Irregular short-period variations in $\delta\dot{\Phi}$ somewhat obscure the smooth average electron-density characteristics in the region of the satellite-to-ground path. From DM/CSM measurements of $\delta\dot{\Phi}$, we can obtain knowledge of the irregularity of N along the orbit, limited only by the 10-sec (77-km) resolution provided by the on-board doppler records and the 300-km distance between the spacecraft. Since the ASTP orbit is nearly circular, the irregular variations due to $N_c\dot{z}_c$ will be small. The possibility also exists that the DM/CSM ionospheric doppler variations can be used to identify clearly the effect of $N_c\dot{z}_c$ and enable us to remove that term from consideration in the DM-to-ground doppler shift.

In computing ionospheric parameters via equation (8) from observations of $\delta\dot{\Phi}$ in the spacecraft-to-ground case, knowledge of the magnitude of the horizontal gradient is essential to an accurate description of the ionospheric electron content between the transmitter and the receiver. Although the single measurement of $\partial N/\partial x$ at the orbital height gives no direct information about the vertical profile of $\partial N/\partial x$, it may yet be more important since the integral $[\partial\tilde{N}/\partial x]$ is weighted by the height z.

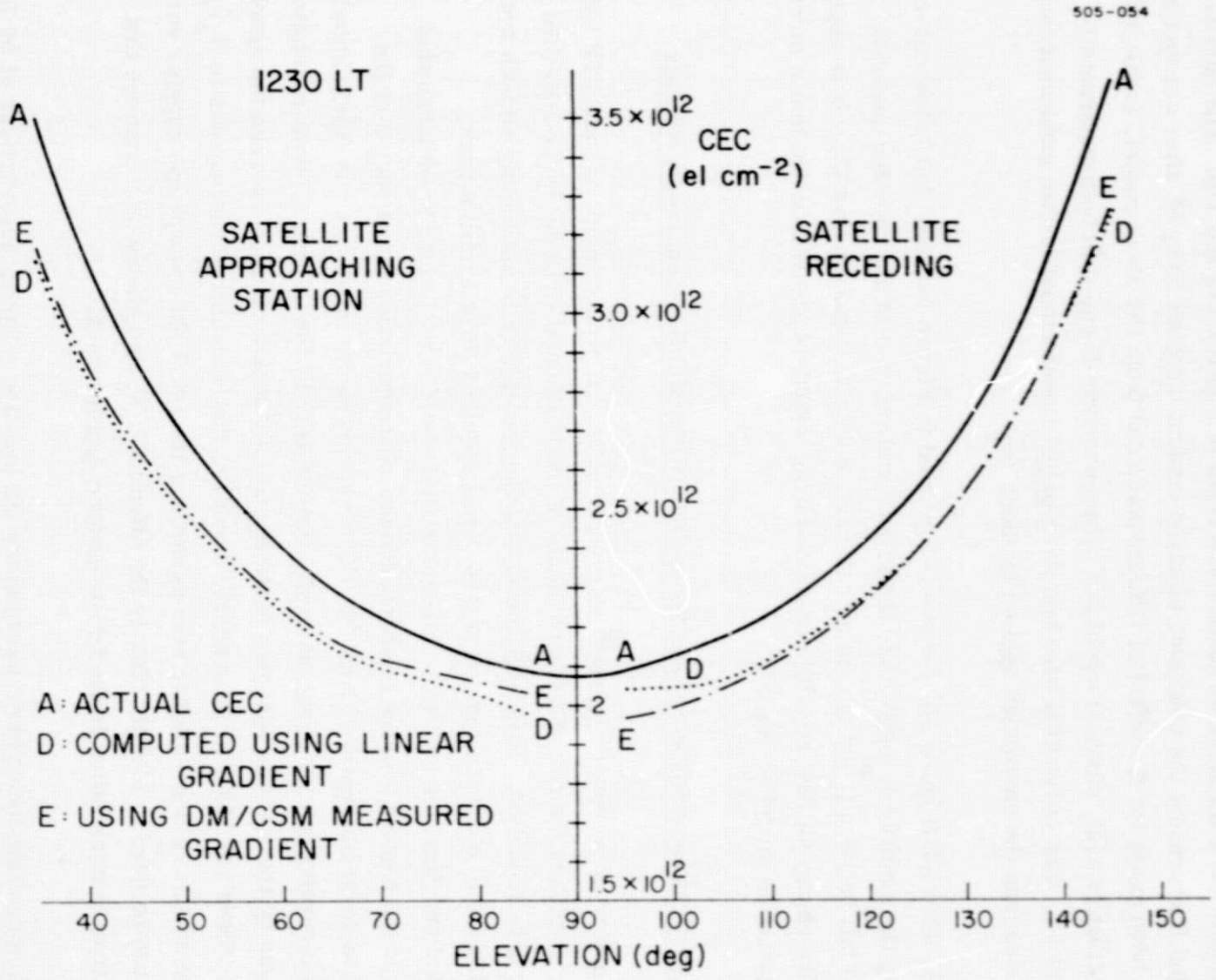

Figure 11a. Continuation of Figure 9a.

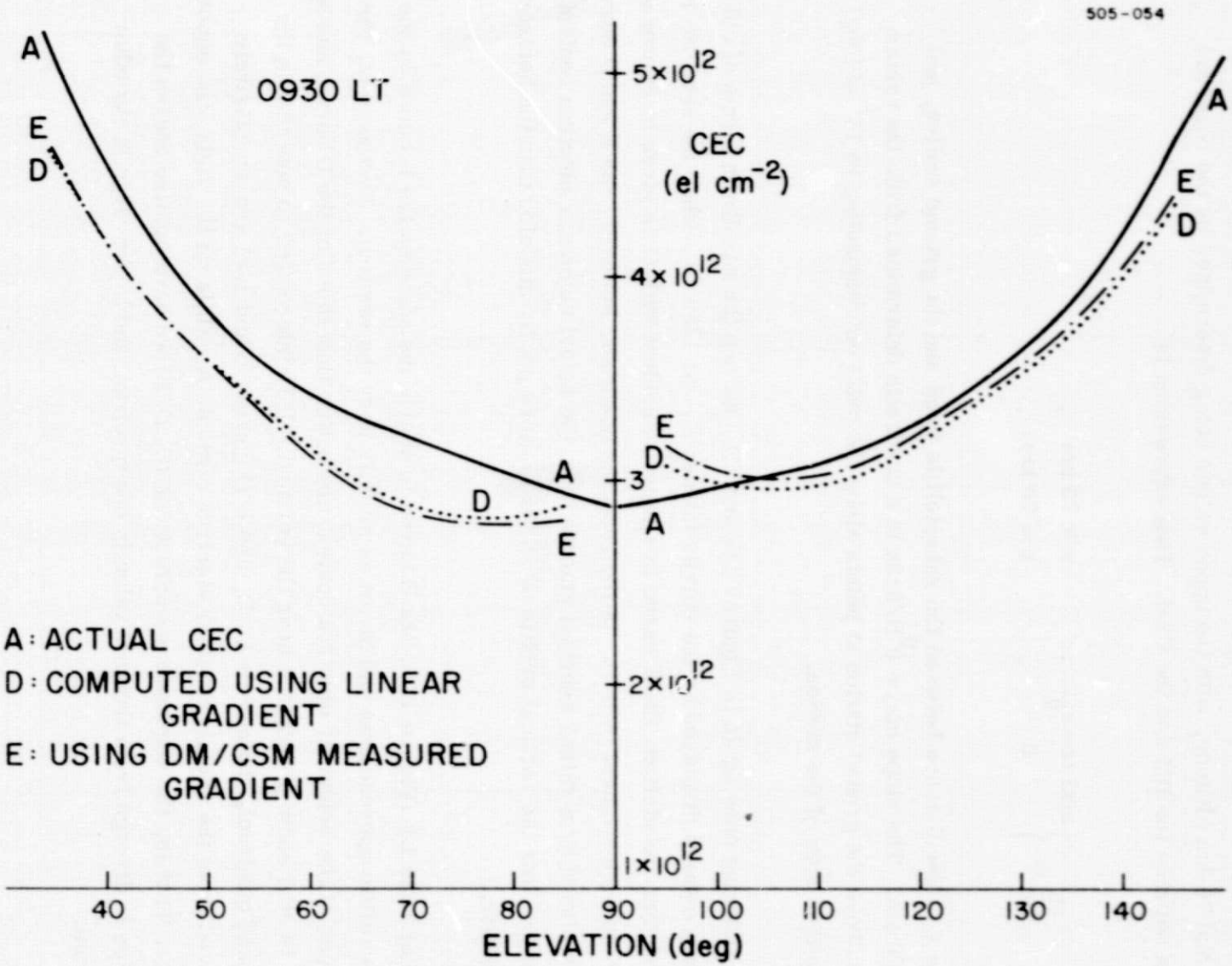

Figure 11b. Continuation of Figure 9b.

To demonstrate what we expect to achieve from the aloft gradient measurement in terms of inversion accuracy, we have again used a linear profile of $\partial N/\partial x$ between 221- and 70-km altitude, with the upper values being determined by the observed $\partial N/\partial x$ between the DM and the CSM. That expression is

$$\frac{\partial N}{\partial x} = \begin{cases} a(x)\ (z - z_0) \ , & z \geq 70 \text{ km} \ , \\ 0 \ , & z \leq 70 \text{ km} \ , \end{cases}$$

where x is the distance between the subsatellite point and the ground station, and $z_0 = 70$ km. The slope $a(x) = \partial^2 N/\partial z \partial x$ is a quadratic determined from the values taken above the ground station at points along the orbit corresponding to 15° of longitude either side of the station.

Referring once again to Figures 11a and 11b, we see the results in terms of columnar electron content displayed by the curves labeled E. At 1230 LT, when the satellite is approaching the station, the E curve is almost coincident with C as given in Figure 9a and is an improvement over D. In the receding quadrant, however, the E and D curves are displaced by a rather constant amount from the actual columnar electron content, suggesting that the vertical profile of $\partial N/\partial x$ is more poorly modeled than the horizontal variability.

For 0930 LT (Figure 11b), the E curve is nearly the same as the D curve on the left (satellite approaching) and diverges slightly near the vertical. On the right, the E values of the columnar electron content are better than those of the D curve, and again there is still some divergence near the vertical. It is interesting to note that in the left-hand quadrant, the curves C, D, and E (Figures 9b and 11b) are successively removed from the actual columnar electron content, A, while on the right, the opposite is true. That is, the sequence of corrections (C, D, E) we have applied causes the solution to diverge from the real value in one quadrant and to converge in the other quadrant.

5. CONCLUSIONS

The analysis of the expected DM-to-CSM differential doppler shifts indicates that a measurement accuracy of 1 to 10% in the value of the horizontal electron-density gradient at 221-km altitude can be achieved. The accuracy increases with the gradient amplitude and is sufficient in each case cited to account adequately for the ionospheric frequency shift in the DM/CSM link, which must be removed for the gravitational experiment. Possible exceptions (where the accuracy of $\overline{\partial N}/\partial x$ is insufficient) are at the nighttime minimum of electron density and in the presence of large temporal variations in N along the radio path.

In the case of ground-based observations near the orbital plane, we have identified some possible effects of the horizontal gradient $\partial N/\partial x$ on the received differential doppler shift and have successfully applied a simple method of compensating for the presence of horizontal gradients in the solution for space-to-ground columnar electron content. In the two cases considered, it was possible to reduce the gradient-associated error in the columnar electron content by approximately one-half by introducing a simple, linear, vertical-profile model of $\partial N/\partial x$. A more appropriate gradient model with more horizontal and vertical details should result in an overall accuracy of 5 to 10% in the columnar electron content. In our simulation, the horizontal-gradient measurement at the ASTP altitude employed in conjunction with a linear model of the gradient profile gives essentially the same correction as does the a priori linear model. The rms difference between the simulated columnar electron content and that given by curve E in figures 9 and 11 is 6.5% in the 1230 LT case and 7.5% for the 0930 LT case.

The results of these numerical experiments, performed under assumed idealized conditions, cannot yet be applied broadly without further consideration of the effects we have neglected, especially at satellite altitudes different from the ASTP orbital height. We hope to perform more simulations that will include the earth's magnetic field, the time variability of N, and the effects of out-of-plane motion ($\dot{y}_c \neq 0$) if time permits.

6. ACKNOWLEDGMENTS

We acknowledge the support given by Dr. G. C. Weiffenbach, who provided technical guidance throughout the effort. The encouragement given by Dr. Erwin R. Schmerling was instrumental in starting this project. Helpful discussions with Prof. Ya. L. Al'pert at Izmiran are also acknowledged.

The authors wish to thank Mr. Thomas I. S. Boak III for his programing effort and for the numerical computations that he performed.

7. REFERENCES

Al'pert, Ya. L. (1963). The refraction and doppler shift of radio waves emanating from an artificial earth satellite in a three dimensional nonhomogeneous ionosphere, Geomagn. and Aeron., vol. 3, pp. 505-511.

Al'pert, Ya. L. (1965). On the results of ionosphere investigations with the help of coherent radiowaves emitted by satellites, in Space Research V, edited by D. G. King-Hele, P. Muller, and G. Righini, published by North-Holland Publ. Co., Amsterdam, pp. 652-686.

Al'pert, Ya. L., and V. M. Sinel'nikov (1965). Altitude-time distribution of electron concentration in the outer ionosphere and its stratified-inhomogeneous disturbance, I, Geomagn. and Aeron., vol. 5, p. 209-219.

Al'pert, Ya. L., L. N. Vitishas, and V. M. Sinel'nikov (1965). Altitude-time distribution of electron concentration in the outer ionosphere and its stratified-inhomogeneous disturbance. II, Geomagn. and Aeron., vol. 5, pp. 766-767.

Chapman, S. (1931). The absorption and dissociative or ionizing effect of monochromatic radiation in an atmosphere on a rotating earth, Proc. Phys. Soc. (London), vol. 43, pp. 26-45.

Grossi, M. D., and R. H. Gay (1975). Doppler measurements of the ionosphere on the occasion of the Apollo-Soyuz Test Project. Part I: Computer simulation of ionospheric-induced doppler shifts. Smithsonian Astrophysical Observatory Spec. Rep.

Hibberd, F. H., and J. A. Thomas (1959). The determination of the electron distribution in the upper ionosphere from satellite doppler observations, Journ. Atmos. Terr. Phys., vol. 17, pp. 71-81.

Kelso, J. M. (1964). Radio Ray Propagation in the Ionosphere, McGraw-Hill Book Co., New York, 408 pages.

Odom, D. (1975). Private communication.

Tyagi, T. R. (1974). Determination of total electron content from differential doppler records, Journ. Atmos. Terr. Phys., vol. 36, pp. 1157-1164.